Astron. Astrophys. 337, 729–738 (1998)

ASTRONOMY
AND
ASTROPHYSICS

ISO far-IR spectroscopy of the black hole candidate GRS 1915 + 105⋆

Christoph Winkler[1] **and Norman Trams**[2]

[1] Space Science Department of ESA, Astrophysics Division, ESTEC, 2200 AG Noordwijk, The Netherlands
[2] Space Science Department of ESA, Astrophysics Division, ISO Science Operations Centre, E-28080 Madrid, Spain

Received 2 March 1998 / Accepted 9 June 1998

Abstract. We have observed the black hole candidate and Galactic superluminal source GRS 1915+105 with ISO LWS and SWS in March 1996 and March 1997 when the source was at fairly low X-ray and radio flux levels. If the source is associated with a dense molecular cloud, then corresponding far-IR continuum and line fluxes should be easily detectable and the data should constrain models for accretion from ISM (Maloney et al. 1997). The integrated fluxes in the SWS (2.3 - 45.2 μm) and LWS (43.2 - 195.6 μm) are 2.5×10^{-17} and 8.9×10^{-17} W/cm^2, respectively. The continuum above 50 μm is well represented by thermal black body radiation of T = (25.9 $\pm$ 0.8) K, modified by a dust emissivity component $\epsilon \sim \lambda^{-1.5}$. This can be indicative of a dust cloud with radius $r_{Dust} \sim 0.3$ pc, and mass $M_{Dust} \sim 5.5\ M_{\odot}$. However, we do not detect significant line emission in the background subtracted LWS spectrum of GRS 1915+105, as predicted by Maloney et al. (1997) for far-IR lines of the ambient ISM excited by compact objects, and the 3σ upper limits are below 7.5 to 9.6 $\times$ 10^{-20} W/cm^2 for prominent lines as [OI], [OIII], [NII] and [CII]. The non-detection of fine-strucure lines implies that either GRS 1915+105 is not embedded in a dense molecular cloud or, if the source would be indeed close to such a cloud, the source X-ray luminosity averaged over the past few hundred years is significantly below 10^{37} erg/s so that line intensities are low. We conclude that the far-IR continuum emission from the source region, with T = 26 K not unusual for the ISM, is most likely not related to GRS 1915+105 and that most probably GRS 1915+105 is not surrounded by dense ISM, so that the lack of detected line emission is a consequence of the absence of material suitable for irradation.

Key words: stars: individual: GRS 1915+105 – ISM: clouds – infrared: ISM: continuum – infrared: ISM: lines and bands – infrared: stars

Send offprint requests to: C. Winkler, (cwinkler@astro.estec.esa.nl)

⋆ Based on observations with ISO, an ESA project with instruments funded by ESA Member States (especially the PI countries: France, Germany, the Netherlands and the United Kingdom) with the participation of ISAS and NASA.

1. Introduction

The hard X-ray transient GRS 1915+105 was discovered in 1992 by the WATCH/GRANAT all-sky monitor (Castro-Tirado et al. 1992). The source is characterized by its extreme and erratic variability: following periods of high activity after its detection, GRS 1915+105 became strongly variable again during 1995 to 1996 as monitored by GRANAT/WATCH, RXTE, BATSE and in the radio (Sazonov & Sunyaev 1995a, 1995b, 1995c, 1995d, Harmon et al. 1995, 1995a, Zhang et al. 1995, Morgan et al. 1996, Zhang et al. 1996, Ghigo et al. 1995, Waltman et al. 1995).

During December 1996 GRS 1915+105 had reached highest flux levels (reaching at time 500 mCrab) in the BATSE 20 - 100 keV range with a hard ($-$ 2.8) power law spectrum, while RXTE data (2 - 10 keV) showed count rates and variability at lowest levels during the same time intervals. The source remained active up to at least Spring 1997 and RXTE reported bright flares in May 1997 (up to 800 mCrab, 2 - 12 keV) ending a long interval of steady hard X-ray emission since December 1996 as well as an increase of day-to-day variability in conjunction with radio flares observed in April 1997 (Remillard et al. 1997, Robinson et al. 1997). Most recently, during 2nd half of 1997, GRS 1915+105 has undergone new extraordinary X-ray/radio outbursts.

We briefly summarize the observational status of this source whose nature yet remains unclear.

1.1. Counterparts

Counterparts to the source have been detected at hard X-rays with SIGMA and CGRO/BATSE (Finoguenov et al. 1994, Harmon et al. 1992), with fluxes at the (150 $\pm$ 20) mCrab level in the 35 - 70 keV range in September 1992 and a power law slope of $-$ 2.5 $\pm$ 0.3 (35 - 250 keV); at soft X-rays with ROSAT HRI (Greiner 1993); in the radio with fluxes of 7 mJy at 20 cm, about 2 - 5 mJy at 3.6 cm, and in the infrared: J(1.25 μm) $\sim 18^m$, H(1.65 μm) $\sim 16^m$, K(2.2 μm) $\sim 14^m$ (Mirabel et al. 1994). Rapid variability indicates that the radio source must be compact in its nature. Day to day variations of 1.2^m of the IR flux have been seen in 1994 (Mirabel et al. 1994), but not in 1995 during similar hard X-ray/radio flaring (Eikenberry & Fazio 1995), and

the 20 cm radio flux is possibly correlated with 20 - 100 keV BATSE data (Mirabel et al. 1994). A probable counterpart was observed in the optical wavelength range (m_I = 23.4, Boër et al. 1996).

In August 1992, when BATSE observed an increase in intensity (Harmon et al. 1992), soft gamma-ray transient events (each lasting less than 1 s) were reported by BATSE (Kouveliotou et al. 1993) from a region consistent with the known soft gamma-ray repeater SGR 1900+14, fairly close to GRS 1915+105. It is possible - however not proven - that GRS 1915+105, SGR 1900+14 and the 3 SGR events observed by BATSE originate in the same source (see Mirabel et al. 1994, Grindlay 1994, Mirabel & Rodriguez 1996 and Castro-Tirado 1996 for discussion). The probability of coincidental superposition of GRS 1915+105 and the BATSE SGR is 1% (Mirabel et al. 1994).

Multiwavelength observations (IR and mm) showed that GRS 1915+105 is at a kinematic distance of (12.5 $\pm$ 1.5) kpc (Chaty et al. 1996), behind the core of a molecular cloud (Grindlay 1994, Durouchoux et al. 1994) at (9.4 $\pm$ 0.2) kpc with a total hydrogen column density $N_H = (4.7 \pm 0.2) \times 10^{22}$ cm^{-2} - consistent with $N_H = \sim 5 \times 10^{22}$ cm^{-2} derived earlier from ROSAT X-ray data (Greiner et al. 1994) - and a visual absorption $A_V = 26.5^m \pm 1^m$ (Chaty et al. 1996).

Major progress in understanding the nature of the source has been found recently using simultaneous or near-simultaneous observations at different wavelengths: Near-infrared (J, H, K) emission was observed to be delayed with respect to radio emission (3.5, 9, 20 cm) by 2 - 5 days suggesting the appearance of a warm dust component coming from a region which can not come from the cooler component of an accretion disk with a typical size of a few light-seconds. The enhanced infrared emission was close to 10% of its X-ray luminosity (Mirabel et al. 1996). Evidence for a hard X-ray/radio anticorrelation on timescales of a few days is found in a sense that hard X-ray data dip or decrease after an ejection event or radio flare which can be attributed to ejected plasmoids (Harmon et al. 1997) suggesting that accreted material is feeding the jets. Simultaneous near-IR and RXTE data (Eikenberry et al. 1998) rule out thermal reprocessing of X-ray flux as the source of IR flux. Data are consistent with a scenario where material from the inner accretion disk producing IR flux via synchrotron emission is ejected providing evidence for the first time that jets are linked to the inner disk (Eikenberry et al. 1998). Simultaneous observations in the X-ray, infrared and radio wavelengths show that during episodes of rapid disappearance and replenishment of the inner accretion disk, relativistic plasma clouds in form of IR and radio synchrotron flares are being ejected (Mirabel et al. 1998).

1.2. Jets, superluminal motions and accretion disk

VLA 3.5 cm observations obtained in 1994 (and later in 1996) shortly after a strong radio outburst (>1 Jy) showed bright radio condensations moving at apparent superluminal speed (Mirabel & Rodriguez 1994, 1995, Mirabel et al. 1996) identifying that source as the first microquasar in our Galaxy.

The existence of near-infrared jets was reported in July 1995 by analysing asymmetries in IR images (Sams et al. 1996) but not confirmed in June 1996 (Sams & Sunyaev 1996a, Eikenberry & Fazio 1997). No evidence for extended jets was found either in 20 cm observations of the surroundings of GRS 1915+105, but two radio sources (also bright in the IRAS catalogue) were found located symmetrically at 17′ from the source at a position angle consistent with the one found for the ejected radio condensations (Mirabel & Rodriguez 1996a). This suggests evidence for interaction of the radio jet material with the nearby ISM.

Detailed analysis of RXTE lightcurves obtained in Feb - June 1996 reveal drastic changes in X-ray (2 - 12 keV) fluxes ranging from subseconds to days. The source exhibits quasi-periodic brightness "sputters" with remarkably different spectral behaviour possibly caused by instabilities in the accretion disk. Because these sputters precede radio flare outbursts in two cases, it is therefore argued that superluminal ejections might be related to episodes of large-amplitude X-ray variations (Greiner et al. 1996). The complex spectral-temporal behaviour as observed by RXTE could be explained by rapid removal and slower replenishment of material forming the inner part of an optically thick accretion disk - similar to those associated with dwarf novae (Belloni et al. 1997, 1997a).

1.3. GRS 1915+105: a black hole in a binary system ?

From the infrared magnitudes, color and time variability, Chaty et al. (1996) conclude that GRS 1915+105 has a striking resemblance with SS 433, i.e. it is proposed that GRS 1915+105 is a collapsed massive object with a thick accretion disk in a high-mass binary system. This explanation is also supported by the existence of superluminal jets, so far only known to exist in AGN, believed to harbour black holes. However, K-band spectra obtained after a bright X-ray burst in September 1994 have shown prominent H and He emission lines, not Doppler shifted (in contrast to those observed in SS 433) suggesting that the lines are not originating in beams of energetic particles responsible for the radio lobes (Castro-Tirado et al. 1996), and these authors further conclude that GRS 1915+105 is most likely a low-mass X-ray binary system (see also Mirabel et al. 1997 for discussion on HMXB vs LMXB). Evidence for a possible hot spot orbiting the collapsed companion of a binary system has been claimed from analysis of 3.6 cm radio data (Sept. 95) showing sinusoidal oscillations with a period of 30.2 $\pm$ 0.4 minutes (Rodriguez & Mirabel 1997).

QPO's were detected by RXTE at 0.5 - 100 mHz and 67 Hz and by IRS-P3 around 0.7 Hz (Morgan et al. 1996, Agrawal et al. 1996, Paul et al. 1997) and in the radio with periods in the 20 - 40 min range (Pooley 1996, Pooley & Fender 1997). The 67 Hz QPO would imply a black hole mass of 33 $M_\odot$ if the QPO reflects the rotation frequency of the innermost stable orbit around a non-rotating Schwarzschild black hole (Morgan et al. 1997). Alternatively, the black hole mass would be 11 $M_\odot$ if the 67 Hz feature is caused by g-mode oscillations of the accretion disk (Nowak et al. 1997). The ensemble of power spectra, energy

spectra and light curves obtained by RXTE in 1996 is interpreted as succession of four different emission states where none of the states appears to meet any known "canonical" state of black hole binaries (Morgan et al. 1997). RXTE data show that the source populates two branches in the hardness-intensity diagram with a variety of QPO features and with strong similarities to other X-ray transients like Nova Muscae 1991, GS 1124−68 and GX 339−4 (Chen et al. 1997), and that the source reveals a wide range of transient activity including regular bursts at one minute intervals with secondary and tertiary weaker bursts with soft - to - hard spectral evolution implying a corona-disk configuration of the accretion flow (Taam et al. 1997).

2. Motivation for ISO observations

The existing multiwavelength observational data of GRS 1915+105, its rapid (correlated ?) variations, evidence of a (complex) accretion disk, its possible association with a recurring soft gamma-ray repeater and its possible association with giant molecular clouds make this Galactic black hole candidate a key target for Target of Opportunity observations with ISO SWS and LWS spectrometers covering the 2 - 195 μm range which is yet completely unexplored. Grindlay (1994) discussed a possible astrophysical model in which a compact object, possibly a black hole, is embedded within or close to a giant molecular cloud and fed by spherical accretion. Soft gamma-ray bursts could be explained through thermal instabilities in the accretion flow. It is noted that accretion from giant molecular clouds onto a black hole system has also been proposed for the unusual hard x-ray source 1E1740.7−2942 in the Galactic Centre (Bally & Leventhal 1991) which exhibits a temporal 511 keV annihilation line (Sunyaev et al. 1991) and shows collimated radio jets (Mirabel et al. 1992).

It has been recently shown that the irradation of interstellar matter in the vicinity of compact sources by $\sim$1 keV photons can generate significant fluxes in a number of far-infrared lines such as [OI] 63 μm, [C II] 158 μm, and [Si II] 35 μm, as they are predicted for the Galactic Centre compact sources 1E1740.7−2942 and GRS 1758−258 (Maloney et al. 1997). We note that these two Galactic Centre sources and GRS 1915+ 105 are quite similar in their observational characteristics (e.g. luminosity, spectrum, jets, association with molecular clouds).

If the source is associated with a dense molecular cloud, then, whether the source is fed by direct accretion or via an accretion disk fed by a companion, corresponding far-IR continuum and line fluxes should be easily detectable. The data should then allow to derive important observational constraints on e.g. gas and column density, and should constrain models for accretion from ISM (Maloney et al. 1997).

Imaging photometry in the K-band revealed rapid infrared flares on time-scales of less than an hour (Fender et al. 1997) which are strikingly similar to those flares regularly observed in the radio at 15 GHz, suggesting a common emission process - infrared synchrotron radiation.

3. Observations

Observations of GRS 1915+105 (Table 1) were carried out in 1996 and 1997 using the Long Wavelength Spectrometer (LWS) and the Short Wavelength Spectrometer (SWS) on board ESA's Infrared Space Observatory (ISO) Mission as part of the Open Time programme.

ISO (Kessler et al. 1996) is a helium cooled 60 cm telescope covering the 2.5 - 240 μm wavelength range with 4 focal plane instruments each having a 3′ unvignetted field of view. The LWS (Clegg et al. 1996) with its 80" beam was used in grating mode AOT-LWS01, medium resolution, covering the 43.2 - 195.6 μm wavelength range as fast scans with a spectral sampling of 1/2 of the spectral resolution element 0.29 μm (43 - 90 μm) and 0.60 μm (90 - 195 μm). The SWS (de Graauw et al. 1996) was operated in grating mode AOT-S01, low resolution, covering the full wavelength range from 2.38 - 45.2 μm (bands 1A to 4) at speed 3, i.e. with resolving power 1/4 of the full SWS spectral resolution (of the order of 1000 to 2000). The SWS apertures are 14" × 20" (bands 1 and 2), 14" × 27" (bands 3A - 3D), 20" × 27" (band 3E), and 20" × 33" (band 4).

The source position is given from the radio counterpart location at α_{1950} = $19^h12^m49.97^s$, δ_{1950} = $10°51'26.8''$, accuracy: $\pm$ 1.5″ (Mirabel et al. 1994). The LWS spectra obtained at the source position were supplemented by an off-source (background) measurement 11.5′ south of the source position (Table 1). No spatial hopping was performed for the SWS measurements: the background contribution from mainly zodiacal light may contribute to the SWS data on the order of about 0.3 Jy (v.d. Hucht et al. 1994).

In this paper we report detailed results obtained from the LWS data, and preliminary results obtained from the SWS data. The data reduction and analysis of the SWS data is on-going and detailed SWS results will be presented in a forthcoming publication.

4. Data analysis and results

4.1. LWS spectra

Raw data from all three LWS observations (1996/1997 on-source and 1996 off-source) were processed with the pipeline processing version 6.0 . The resulting auto analysis data (AAR) were analysed using the ISO Spectral Analysis Package (ISAP) V1.3 and included the following processing steps per LWS spectrum (observation): (i) remove bad AAR data and outliers (typically 27%); (ii) average all 10 detectors individually by keeping the default LWS grating resolutions; (iii) defringe detectors SW5 to LW5 which show significant sinusoidal fringing due to interference within the instrument; (iv) shift all individual scans in flux using the spectrum of detector LW2 (110 - 130 μm) as normalization reference[1]; (v) rebin the entire spectrum to 0.1

[1] We used LW2 as normalization reference and not detectors SW3 or SW4, usually recommended as reference, because the spectra from the latter detectors were not of high enough quality while LW2 showed a reasonable S/N ratio. In addition, memory effects for this source are small.

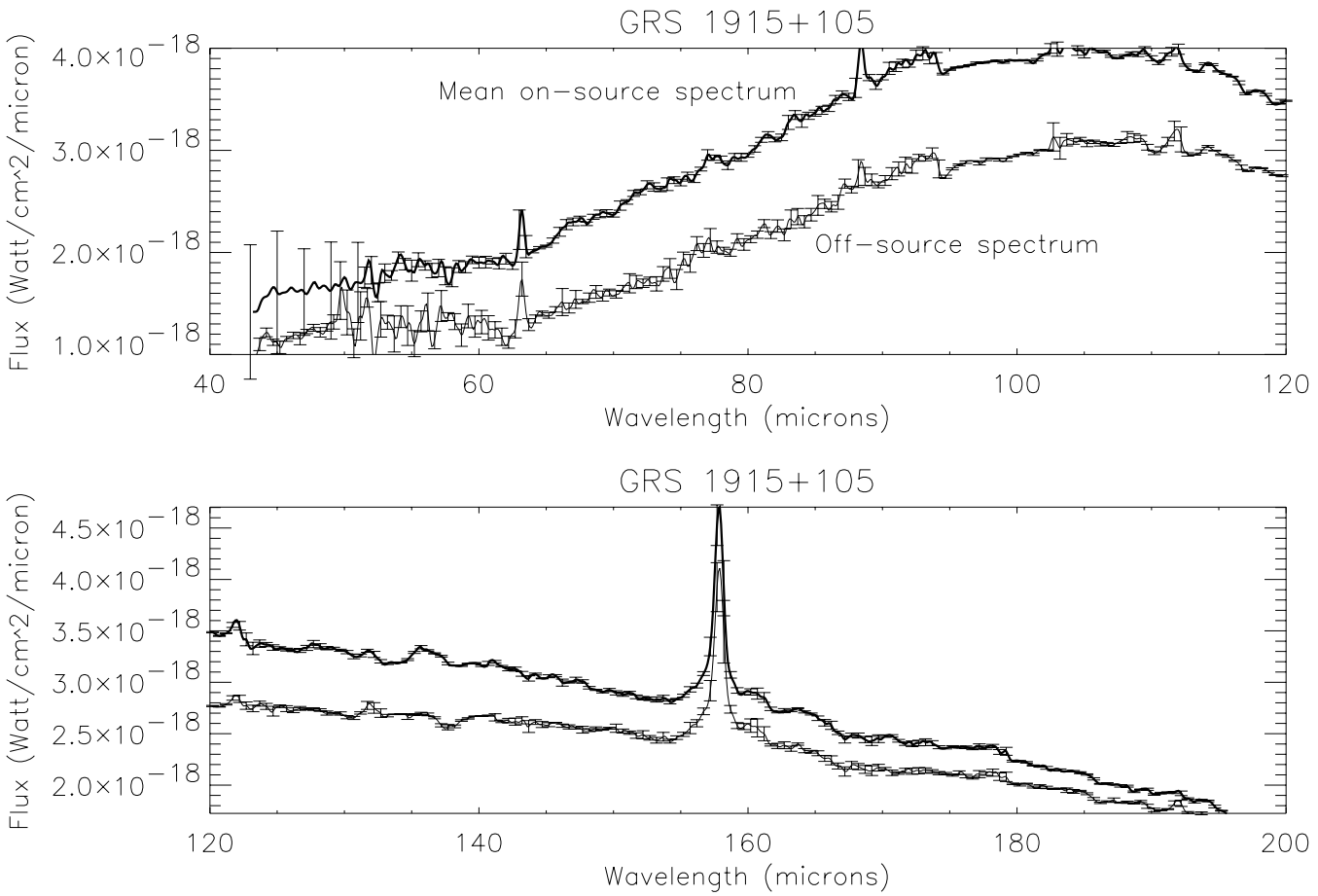

Fig. 1. Mean (1996 + 1997) on-source LWS spectrum (thick line, top curve) of the sky region containing GRS 1915+105 and including sky background, and off-source background spectrum (thin line, bottom curve). For clarity only every 5^{th} error bar is plotted. See text for details.

Table 1. Journal of LWS and SWS observations of GRS 1915+105

Start Date (UTC, h:m:s)	End Date (UTC, h:m:s)	RA (J2000)	DEC (J2000)	Instrument/Mode	Notes
9 Mar 1996 15:36:32	9 Mar 1996 16:43:53	19h 15m 11.5s	+10° 56′ 44.9″	LWS/AOT 1	On-source
9 Mar 1996 16:45:01	9 Mar 1996 17:52:21	19h 15m 11.7s	+10° 45′ 18.1″	LWS/AOT 1	Off-source
9 Mar 1996 17:53:29	9 Mar 1996 18:51:11	19h 15m 11.5s	+10° 56′ 44.9″	SWS/S01	On-source
9 Mar 1997 18:29:35	9 Mar 1997 19:27:09	19h 15m 11.5s	+10° 56′ 44.9″	SWS/S01	On-source
9 Mar 1997 19:27:51	9 Mar 1997 21:22:13	19h 15m 11.5s	+10° 56′ 44.9″	LWS/AOT 1	On-source

μm resolution and, finally (vi) smooth it with a 0.35 μm wide Gaussian.

Because of the expected weak signal we have combined both 1996 and 1997 on-source observations (Table 1) into one mean on-source spectrum. The validity of this approach has been verified by inspecting the position angle of the 1996 and 1997 SWS observations performed together with the LWS observations: being one year apart, the position angles of the SWS aperture are almost identical (100.42° in 1996 and 100.95° in 1997) which means that the same area on the sky has been observed in 1996 and 1997.

Fig. 1 shows the mean (1996 + 1997) on-source spectrum including sky background (thick line), and the off-source background spectrum (thin line) for comparison. The steps at 94 and 103 μm in both spectra are due to imperfect averaging at boundaries between LWS detectors SW5 and LW1, and LW1 and LW2, respectively. The errors on the mean spectrum from the source region were calculated using standard error propagation for the flux errors on the individual spectra from 1996 and 1997 observations. For the mean on-source spectrum at wavelengths in the 52 - 195 μm range, the relative flux ratio per bin defined as $F = (flux_{1997} - flux_{1996})/flux_{1997}$ is on average $< F >$ = (− 2 ± 1)% within a range between + 25% and − 10% showing that the overall source flux remained fairly constant for the two observations. However, below 52 μm we find on average $< F >$ = (− 79 ± 38)% with $flux_{1997}$

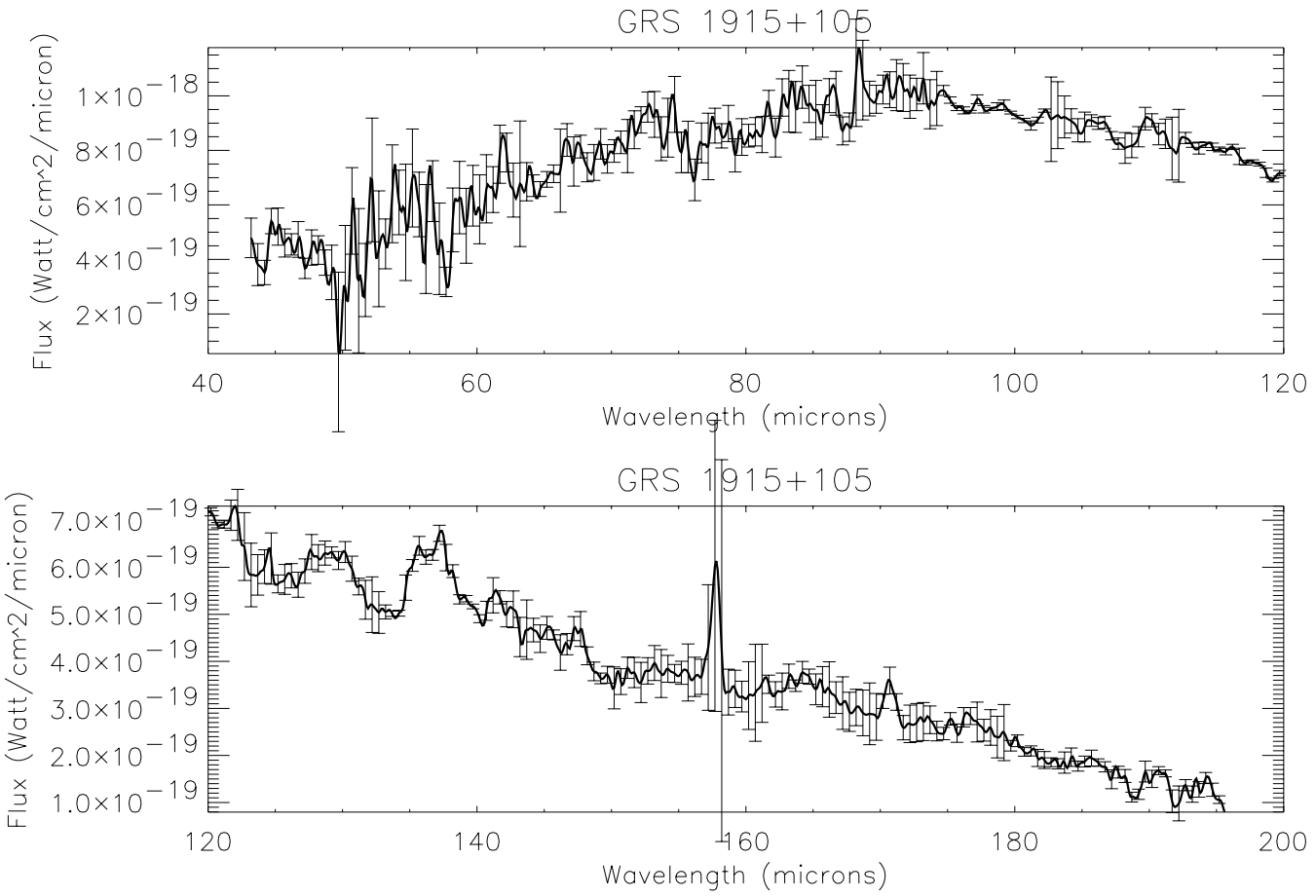

Fig. 2. Mean (1996 + 1997) background subtracted LWS spectrum of the sky region containing GRS 1915+105. For clarity only every 5^{th} error bar is plotted.

Table 2. Emission lines identified in the spectra of the on-source region including sky-background (Fig. 1, top curve) and off-source region (Fig. 1, bottom curve). ΔV denotes the offset between the fitted and identified wavelengths.

Spectrum in Fig. 1	Fitted line center (μm)	FWHM (μm)	Identification (μm), ID	Flux (10^{-19} W/cm^2)	ΔV (km/s)	SNR
top	63.1806±0.0166	0.37±0.02	63.1837, [OI]	1.77±0.25	− 15	8.6
top	88.4259±0.0182	0.51±0.02	88.3560, [OIII]	2.56±0.29	237	9.1
top	157.8314±0.0083	1.10±0.01	157.7410, [CII]	21.05±0.49	172	29.4
bottom	63.1729±0.0208	0.47±0.02	63.1837, [OI]	2.40±0.33	− 51	7.7
bottom	88.4141±0.0479	0.74±0.05	88.3560, [OIII]	2.08±0.43	197	4.2
bottom	157.8522±0.0098	1.26±0.01	157.7410, [CII]	20.64±0.49	211	26.9

dropping to 50% (at 45 μm) of the value observed one year earlier. Larger error bars below 52 μm (SW1 detector) in Fig. 1 indicate this systematic deviation around the mean on-source spectrum. A variability of the source in that wavelength band can not be the cause for this behaviour as this change in flux is not supported by our contemporaneous SWS data below 43 μm. Instead we consider instrument related effects to explain the systematic difference: On revolution 150 (15 April 1996) the biases on detectors SW1 and SW2 were increased, i.e. the responsitivity for earlier observations was lower and data more noisy. Furthermore, SW1 intrinsically gave problems with the repeatability of a recorded spectrum. This detector shows strong memory effects, and therefore the signal depends on the source observed previously.

In each of the spectra shown in Fig. 1 we identify three emission lines at $\lambda\lambda$ = 63, 88, and 158 μm with high significance which have been fitted by Gaussians with results shown in Table 2.

The systematic errors, as derived from the analysis of the LWS in-flight calibration and performance for wavelength and absolute flux are 0.046 μm and $\sim$20% for bright sources, respectively (Burgdorf et al. 1997a, 1997b). The 3σ wavelength

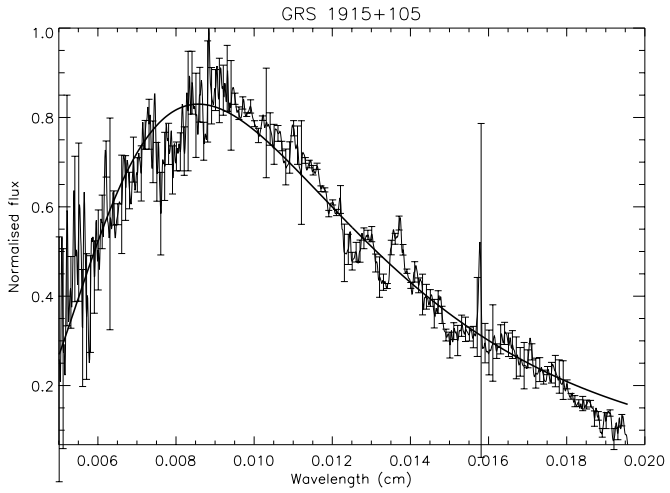

Fig. 3. Black body spectrum with T = (25.9 ± 0.8) K, modified by a dust emissivity component $\epsilon \sim \lambda^{-1.5}$ fitted to mean background subtracted LWS spectrum ($\lambda > 50\mu$m).

error (0.14 μm or v_{rad} = 420 km/s at 100 μm) shows that the identified emission lines are fully compatible with the fitted lines and consistent with v_{rad} = 0 km/s. We note that v_{rad} of GRS 1915+105 with respect to the local standard of rest is − 8.5 km/s.

From the mean LWS on-source spectrum (Fig. 1, top curve) we finally subtract the off-source LWS spectrum (Fig. 1, bottom curve) and Fig. 2 shows the background subtracted spectrum of the sky region containing GRS 1915 + 105. The total flux of the background subtracted spectrum, integrated between 43.2 μm and 195.6 μm is 8.9×10^{-17} W/cm^2, and the averaged intensity is 27.8 Jy.

The shape of the continuum after background subtraction can be described by thermal processes, although it is significantly narrower than a single black body spectrum. We have fitted the data above 50 μm with a black body spectrum which has been modified with a dust emissivity component $\epsilon \sim \lambda^{-1.5}$. The best fit results in a temperature of T = (25.9 ± 0.8) K (Fig. 3). However, the exact wavelength dependency of the dust emissivity ϵ is not known. Therefore we also fitted the data above 50 μm with a black body spectrum modified with a dust emissivity component $\epsilon \sim \lambda^m$, with m = 1, 2. The best fits result in temperatures of T = (28.3 ± 0.9) K for m = 1 and T = (23.8 ± 0.7) K for m = 2.

From Fig. 2 we conclude that no significant line emission can be detected in the net source spectrum. This is already evident from the results in Table 2 where the differences in line fluxes are compatible with zero: $\Delta f_{[OI]} = (-0.62 \pm 0.41)\ 10^{-19}$ W/cm^2, $\Delta f_{[OIII]} = (0.49 \pm 0.51)\ 10^{-19}$ W/cm^2, and $\Delta f_{[CII]} = (0.41 \pm 0.70)\ 10^{-19}$ W/cm^2. We derive 3σ upper limits on line fluxes of various expected lines by calculating $F_{u.l.} = 3 \cdot RMS \cdot \delta\lambda$, where RMS is the root mean square noise and $\delta\lambda$ is the resolution element of the LWS (0.29 μm below 90 μm and 0.60 μm above 90 μm). The results are shown in Table 3.

Table 3. 3σ upper limits on emission line fluxes of background subtracted spectrum shown in Fig. 2.

Wavelength (μm)	ID	$F_{u.l.}$ (10^{-19} W/cm^2)
51.8	[OIII]	< 0.96
63.2	[OI]	< 0.96
88.4	[OIII]	< 0.76
121.9	[NII]	< 0.83
145.5	[OI]	< 0.75
157.7	[CII]	< 0.75

4.2. SWS spectra

Data have been processed using the Interactive Analysis (IA) software at the ISO Data Centre (MPE, Garching). The data processing and detailed analysis of the SWS spectra is on-going and results will be reported in a forthcoming paper. Our preliminary analysis indicates that the source is very weak in both observations. During the two observations in 1996 and 1997, the position angles of the observations were almost identical (see above). We have therefore combined both spectra into a mean SWS spectrum of the sky region containing GRS 1915+105.

The integrated flux over the entire SWS range (2.3 - 45.2 μm) of the mean spectrum is 2.5×10^{-17} W/cm^2, and the averaged intensity is 1.1 Jy. As we currently observe residual contamination of data from band 4 ($\lambda > 29.5$ μm) due to glitches, we therefore also report integrated fluxes and averaged intensity from band 1 - 3 data only (2.3 - 29.5 μm), which are 1.66×10^{-17} W/cm^2, and 0.5 Jy, respectively.

We convolved the short wavelength data of the mean SWS spectrum with broad band filters K (λ_0 = 2.83 μm, FWHM = 0.38 μm) and L (λ_0 = 3.81 μm, FWHM = 0.65 μm) and obtain the following (reddened) magnitudes: 11.9^m (K) and 8.6^m (L). The effects of interstellar extinction in the SWS wavelength range have been derived by Genzel et al. (1998) for the Galactic Centre but it is likely that the derived extinction curve is more widely applicable (Lutz et al. 1996). Using $A_V = 26.5^m$ (Chaty et al. 1996), R_V = 3.1 and interpolating the extinction curve derived by Genzel et al. (1998) for K and L wavelengths, we obtain dereddened magnitudes K = 10.0^m and L = 7.3^m, respectively.

5. Discussion

In this section we will first adress the results obtained from contemporaneous observations at other wavelengths, then discuss the implications of our results from our continuum data and finally discuss those from our line emission data.

5.1. Contemporaneous X-ray and radio data

Our results show the source at fairly low intensity levels in the far-IR wavelength range. We compare them with contemporaneous X-ray and radio data.

5.1.1. Hard X-rays (BATSE)

The transient source GRS 1915+105 is regularly monitored by the BATSE instrument on board the Compton Gamma-Ray Observatory CGRO. The light curves obtained by the BATSE Earth occultation method during the epochs of our observations are shown in Fig. 4 and Fig. 5 (Robinson, priv. comm.). The source flux as observed by BATSE (20 - 100 keV) during 20 days preceeding our observations was on average 0.013 photons/(cm^2 s) ($\sim$ 40 mCrab) in 1996 and 0.09 photons/(cm^2 s) ($\sim$ 270 mCrab) in 1997, i.e. the source was in March 1997 on average about 7 times brighter than in March 1996 (Robinson, priv. comm.). This flux increase is not seen in our ISO/LWS data. Prior to and during the 1996 observations (Fig. 4), the source was highly variable on short time scales: while exceeding 0.10 photons/(cm^2 s), corresponding to $\sim$ 310 mCrab, during the first half of 09 Mar 1996 (TJD = 10151), the hard X-ray flux suddenly drops during our ISO 1996 observations to only 0.03 photons/(cm^2 s) or $\sim$ 80 mCrab. Prior to and during the 1997 observations (Fig. 5), the source was again highly variable on short time scales: while exceeding 0.20 photons/(cm^2 s), corresponding to $\sim$ 630 mCrab, during the first half of 09 Mar 1997 (TJD = 10516), the flux drops by a factor $\sim$ 4 within 12 hours. During our ISO 1997 observations the hard X-ray flux as reported by BATSE was around 0.05 photons/(cm^2 s) or $\sim$ 150 mCrab. This means that the contemporaneous BATSE data show a relative flux increase in 1997 of + 46%, about at least a factor 2 higher than observed with ISO/LWS (see Sect. 4.1). It has to be noted, however, that the region in Aquila including GRS 1915+105 is very susceptible to the systematic errors in the BATSE Earth occultation analysis, in particular the approximate alignment of the Earth's limbs with the Galactic plane at rising and setting times of the source, rendering the empirical background fitting inadequate at these times (Paciesas et al. 1996). On 09 March 1997 (TJD 10516), both Earth limbs were almost parallel to the Galactic equator at the position of GRS 1915+105 (Robinson, priv. comm.).

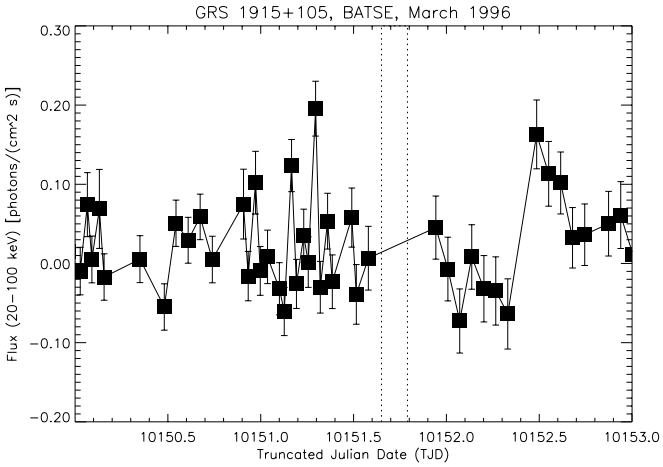

Fig. 4. Lightcurve of GRS 1915+105 obtained by BATSE on board CGRO during 8 - 11 March 1996 (Robinson, priv. comm.). TJD 10151 corresponds to 09 March 1996, the time interval of our observations is indicated by the two vertical lines.

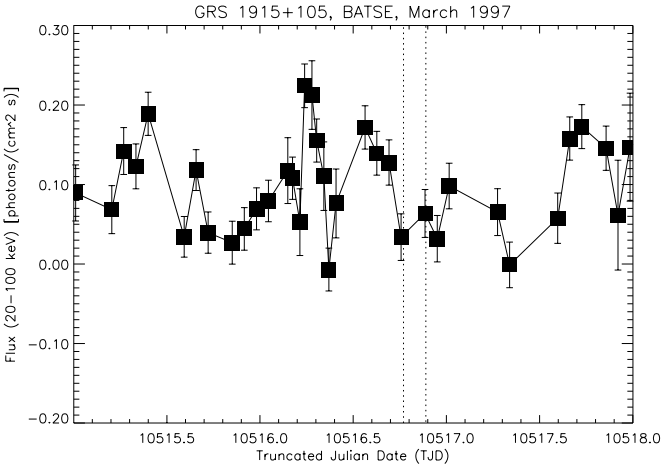

Fig. 5. Lightcurve of GRS 1915+105 obtained by BATSE on board CGRO during 8 - 11 March 1997 (Robinson, priv. comm.). TJD 10516 corresponds to 09 March 1997, the time interval of our observations is indicated by the two vertical lines.

5.1.2. Soft X-rays (RXTE)

During our 1996 observations, RXTE lightcurves (Greiner 1996, Morgan et al. 1997) show chaotic flux variations ranging between 250 and 1000 mCrab (2 - 12 keV). In March 1997, RXTE quick-look data[2] indicate that GRS 1915+105 is declining slowly with less variations and an average flux at around 250 mCrab.

5.1.3. Radio

The source had been monitored in 1995/1996 at 15 GHz (Pooley & Fender 1997). During a long period around March 1996 ($\sim$ 100 days), the flux level was stable and very low (below 0.02 Jy). In contrast to the hard X-ray variability, the radio flux[3] at 2.25 GHz and 8.3 GHz remained fairly constant between TJD 10470 (end Jan 1997) and TJD 10560 (end April 1997) with low fluxes of 10 mJy (8.3 GHz) and 15 mJy (2.25 GHz).

We conclude from this section that contemporaneous observations at hard and soft X-rays in general and at radio wavelengths in particular indicate that the source was relatively low in intensity too. However, we note that the X-ray intensity fluctuations, in particular the rapid stochastic soft X-ray flux variations as observed by RXTE in 1996 do not show immediate impact on far-IR fluxes on the level of the observed sensitivity. As will be discussed in Sect. 5.3, this can be understood by the thermal response time (i.e. cooling time) of the ambient medium which is of the order of 100 years (Maloney et al. 1997).

[2] $http://space.mit.edu/XTE/xte\_anno.html$
[3] $http://www.batse.msfc.nasa.gov/multiwave/$

5.2. Continuum emission

We assume in the following section that GRS 1915+105 is surrounded by a dense molecular cloud.

5.2.1. Bondi-Hoyle accretion

The close vicinity of dense molecular clouds to GRS 1915+105 (Durouchoux 1994, Grindlay 1994, and Chaty et al. 1996) may give rise to Bondi-Hoyle accretion from the molecular cloud onto the compact object as it moves through the dense interstellar medium. The Bondi-Hoyle accretion luminosity (in units of erg/s) is

$$L_{accr} = 2.3 \times 10^{36} \cdot \eta \cdot m_{BH}^2 \cdot v_r^{-3} \cdot n$$

(Bally & Leventhal 1991), with X-ray production efficiency η, total gas density n [in units of 10^4 cm^{-3}], black hole mass m_{BH} [in units of $M_\odot$], and source velocity v_r relative to the ISM [in units of 10 km s^{-1}].

Integrating the LWS spectrum (43.2 - 195.6 μm) we obtain the total far-infrared luminosity L_{FIR} = $4\pi D^2 \cdot 8.9 \times 10^{-17}$ W/cm^2 = 4.4×10^3 $L_\odot$, assuming D = 12.5 kpc (Chaty et al. 1996). We note that L_{FIR} is up to ∼40% of the mean X-ray (20 - 100 keV) luminosity during outburst varying around ∼10^4 $L_\odot$ (Harmon et al. 1997).

RXTE observations of a 67 Hz QPO would imply a black hole mass of 33 $M_\odot$ if the QPO reflects the rotation frequency of the innermost stable orbit around a non-rotating Schwarzschild black hole (Morgan et al. 1997). Alternatively, the black hole mass would be 11 $M_\odot$ if the 67 Hz feature is caused by g-mode oscillations of the accretion disk (Nowak et al. 1997). We assume a X-ray production efficiency of 10% and a total gas density of at least 10^5 cm^{-3} in the vicinity of GRS 1915+105 (see Sect. 5.3, below).

With a probable mass of the black hole in the range between 11 and 33 $M_\odot$, and assuming that L_{accr} not to exceed L_x, it follows that the object would move in the ISM at a velocity of at least 20 - 40 km/s in order to allow that most of its radiation is powered by Bondi-Hoyle accretion. This is not inconsistent with the observations by Castro-Tirado et al. (1992) who did not detect any Doppler shifts in the near-IR H and He emission lines of GRS 1915+105 and we estimate from their data a typical resolution on $v_{Doppler}$ of the order of ± 150 km/s.

We compare with results on the Galactic Centre source 1E 1740−2942, whose observational characteristics are similar to GRS 1915+105 (see above), and a total gas density n is required to be less than 1.5×10^4 cm^{-3} in order for L_{accr} not to exceed the X-ray luminosity (∼ 3×10^{37} erg/s), and assuming that the compact source (∼ 3 $M_\odot$) is moving in the ISM at 2 km/s (Chen et al. 1994).

5.2.2. Properties of the surrounding heated dust cloud

Our far-IR continuum data can be represented by a black body spectrum modified with a dust component whose emissivity is $\epsilon \sim \lambda^{-1.5}$. Following the modelled radiative transfer in a dust cloud surrounding a central star (Scoville & Kwan 1976), we can estimate the radius of the surrounding cloud. For GRS 1915+105 we assume $L_x \sim 10^4$ $L_\odot$ (see above), and with the fitted equilibrium dust temperature to our continuum data, T_{Dust} = 26 K, the average radius of the surrounding dust cloud can be estimated to $r_{Dust} \sim 0.3$ pc (Scoville & Kwan 1976, Eq.(9)).

Thermal dust emission at a particular wavelength can be used as a measure of the dust mass M_{Dust} (Hildebrand 1983) which is given by

$$M_{Dust} = [F(\nu) \cdot D^2 / B(\nu, T)] \cdot [4 \cdot a \cdot \rho / (3 \cdot Q(\nu)]$$

with $F(\nu)$ = flux density, D = source distance (12.5 kpc), $B(\nu, T)$ = Planck function, a = grain radius, ρ = grain density and $Q(\nu)$ = dust emissivity. With λ = 100 μm and T = 26 K we obtain a dust mass of the assumed nearby cloud of M_{Dust} = 5.5 $M_\odot$, using an average flux density of 29.5 Jy at 100 μm (averaged over the 100 μm IRAS filter), and $[4 \cdot a \cdot \rho / (3 \cdot Q(\nu)]$ = 0.04 g/cm^2 (Hildebrand 1983).

The uncertainties of the calculated cloud parameters (T_{Dust} and r_{Dust}) are largely driven by the wavelength dependency of the dust emissivity ($\epsilon \sim \lambda^m$). We estimate therefore the uncertainty on r_{Dust} using temperatures as obtained in Sect. 4, and using Eq. [9] for m = 1 and 2 from Scoville & Kwan (1976), to obtain 0.18 pc ≤ r_{Dust} ≤ 0.50 pc. The uncertainty on M_{Dust} is largely driven by the errors on F(ν) (see Sect. 4.1), and distance D (see Sect. 1.1) and is estimated to ∼ 35%.

During the analysis of near-IR (H, K) observations of an energetic outburst of GRS 1915+105, Mirabel et al. (1996) assumed that the observed variation of the near-infrared flux is due to the appearance of a dust component in the source spectrum. From their measurements at 1.65 and 2.2 μm they obtain $1.2 \times 10^{-10} M_\odot$ of dust radiating at 2300 K. These authors point out that the mass of cold dust could be orders of magnitudes larger, and that in the near-infrared they just see the "tip of an iceberg" in the vicinity of GRS 1915+105, so that most of the dust should radiate at lower temperature. This hypothesis has been therefore tested and confirmed by our results.

However, we note that the fitted temperature (26 K) to the observed continuum radiation is low, not unusual for the ISM. Dust temperatures used in models by Maloney et al. (1997) to predict far-IR line intensities (see Sect. 5.3) from irradiated dust were always above 50 K. These models were calculated using a smaller (factor 2) column density, but a warmer tail of emission at low wavelengths would still be expected if all of the line of sight column is assumed to arise in a cloud surrounding GRS 1915+105 (Maloney, priv. comm.).

This raises doubts on the validity of our assumption on the existence of a nearby cloud, which will be further discussed in the following section.

5.3. Line emission

5.3.1. $F_{[CII]}/F_{[FIR]}$ cooling ratio

The [CII] fine structure line at 157.71 μm has been previously observed in the Galaxy and in extragalactic sources (see e.g.

Table 4. Predicted line fluxes in the LWS range for two Galactic black-hole candidates and total gas densities n, adopted from Maloney et al. (1997, Table 1) scaled to the distance of GRS 1915+105. Line fluxes are in units of 10^{-19} W cm^{-2}.

Wavelength, ID (μm)	1E 1740−2942 n = 10^4 cm^{-3}	1E 1740−2942 n = 10^5 cm^{-3}	GRS 1758−258 n = 10^3 cm^{-3}	GRS 1758−258 n = 10^4 cm^{-3}
63.2, [OI]	58.7	27.7	9.2	12.5
145.5, [OI]	4.2	1.2	0.9	1.4
157.7, [CII]	20.3	0.3	15.3	2.9

Malhotra et al. 1997). Interstellar C^+ provides via this transition an important cooling mechanism for the ISM. The ratio $F_{[CII]}/F_{[FIR]}$ is a measure of the cooling ratio between gas and dust, where $F_{[CII]}$ is the flux of the [CII] line in W/m^2 and $F_{[FIR]}$ (in W/m^2) is a measure for the dust flux under consideration and is calculated via $F_{[FIR]} = 1.26 \times 10^{-14} \cdot [2.58 \times F_{60} + F_{100}]$, where F_{60} and F_{100} are the flux densities in Jy calculated at 60 and 100 μm (Malhotra et al. 1997).

Using the [CII] (157.71 μm) fluxes obtained from the individual spectra of the on-source and off-source positions (Fig. 1, Table 2), i.e. representing the galactic ISM at (l,b) $\sim$ (45°, 0°), and the continuum folded with the IRAS 60 and 100 μm filter functions, we obtain on average (for on-source and off-source pointings) $F_{[CII]}/F_{[FIR]} \sim 0.9\%$. Previous measurements of $F_{[CII]}/F_{[FIR]}$ in the Milky Way result in $\sim$ 0.3% (Stacey et al. 1985) but they defined $F_{[FIR]}$ via the far-IR continuum integrated over the 72 - 196 μm range. Applying this definition, our $F_{[CII]}/F_{[FIR]}$ becomes on average $\sim$ 0.6% not inconsistent with previous results on the ISM.

ISO-LWS and IRAS observations of the diffuse ISM at 61 different positions (cirrus, galactic line of sights and off-position stellar pointings) show, similar to COBE/FIRAS observations on larger scale, that the [CII] line intensity is strongly correlated with the FIR intensity defined as $I_{FIR} = I_{60} + I_{100} + I_{158}$, where I_λ is the continuum intensity at wavelength λ (Caux & Gry 1997). From our on-source and off-source spectra we obtain on average $I_{[CII]} = 208 \times 10^{-20}$ W/cm^2 and $I_{FIR} = 343$ Jy and our data agree very well with the $I_{[CII]} \propto I_{FIR}$ correlation (Caux & Gry 1997, Fig. 1).

5.3.2. Far-IR lines of the ambient ISM excited by compact sources

Two Galactic black hole candidates, 1E 1740.7−2942 and GRS 1758−258, located close to the Galactic Centre, have been recently investigated by Maloney et al. (1997) in order to predict far-IR line emission from the ambient ISM excited by the compact sources.

The observational evidence for those sources shows that the model developed by those authors is quite applicable for GRS 1915+105 too: The 1E 1740.7−2942 and GRS 1758−258 sources are characterized by a hard X-ray spectrum (photon power law index $\sim$1 between 10 and 100 keV); similar luminosity ($L_x \sim$ few 10^{37} erg/s, 10 - 100 keV); significant absorption column density ($N_H \sim 10^{22..23}$ cm^{-2}); synchrotron radio jets with a time variable central source. Moreover, 1E 1740.7−2942 is physically associated with a molecular cloud and a dominant source of time variable 511 keV annihilation radiation (see Maloney et al. 1997, and references therein). High energy radiation from compact sources will ionize and heat the ambient interstellar medium. The X-ray dissociation region (XDR, see Maloney et al. 1996 and 1997 for detailed discussion) in turn generates UV photons, absorbed by interstellar dust which is heated and re-radiating at far-IR wavelengths.

Predicted line intensities depend on the total hydrogen gas density n, the cloud column density and the X-ray luminosity L_x. Mostly X-ray photons with energies E $\sim$ 1 keV and below are responsible for heating and ionization of the ambient medium and about 10% of the X-ray luminosity L_x should be re-radiated in lines and dust continuum. The predicted line intensities are insensitive to short time-scale variations of L_x, because the cooling time is at least of the order of 100 years (Maloney et al. 1997).

We have adopted Table 1 from Maloney et al. (1997) and scaled their predicted line fluxes for 1E 1740−2942 and GRS 1758−258 to the kinematic distance of GRS 1915+105 (12.5 kpc) and the results are shown in Table 4.

Under the assumption, that the model results for 1E 1740−2942 and GRS 1758−258 are basically applicable for GRS 1915+105, because of very similar observational properties, we can compare our 3σ upper limits (Table 3) with the average of the predicted line fluxes (Table 4) and conclude that very high gas densities ($n \geq 10^5$ cm^{-3}) close to the source would be required to match our results at 157.7 and 145.5 μm. However, even for this case, the predicted [OI, 63.2 μm] line flux is at least an order of magnitude above our upper limits.

In order to further suppress the [OI] line emission relative to the continuum, gas densities in excess of $n > 10^6$ cm^{-3} would therefore be required. This, together with the non-detection of the lines at 145.5 and 157.7 μm, poses a serious problem for the assumption that GRS 1915+105 is indeed physically associated with a nearby dense molecular cloud. The non-detection of the [OI, 63.2 μm] line leads to three options:
(i) GRS 1915+105 is not embedded in or adjacent to a dense molecular cloud, or,
(ii) GRS 1915+105 is embedded in a dense cloud but the average X-ray luminosity on a timescale of a few hundred years is significantly lower than $\sim 10^{37}$ erg/s as used in the model by Maloney et al. (1997), so that the predicted line intensities are quite low, or,
(iii) GRS 1915+105 is embedded in a dense cloud with sufficient high density to suppress the [OI, 63.2 μm] line relative to

the continuum by collisional de-excitation. However, this scenario is unlikely because the cloud would be very unusual, as with the observed column density and cloud radius the cloud would have to be very clumpy with $\sim$ 90% of the mass distributed in clumps with $\geq 10^6$ cm^{-3} density (Maloney, priv. comm.).

We conclude using either one of the first two possibilities, that the far-IR continuum emission from the source region, with T = 26 K not unusual for the ISM, is not related to GRS 1915+105 and that most probably GRS 1915+105 is not surrounded by dense ISM, so that the lack of detected line emissions of fine-structure lines as [OI] and [CII] is simply a consequence of the absence of material suitable for irradation.

Acknowledgements. We thank the referee, P. Maloney, for a critical and thorough review of the paper. We thank C. Robinson and the BATSE team for the permission to use unpublished data. The ISO Spectral Analysis Package (ISAP) is a joint development by the LWS and SWS Instrument Teams and Data Centers. Contributing institutes are CESR, IAS, IPAC, MPE, RAL and SRON. We acknowledge support from the ISO Spectrometer Data Centre at MPE Garching, funded by DARA under grant 50 QI 9402 3. C.W. appreciates the efficient support by D. Kunze/MPE (ISOSDC) in reducing SWS data with the Interactive Analysis (IA) software developed by MPE and SRON Groningen.

References

Agrawal P., Paul B., Rao A., et al., 1996, IAU Circ. 6488
Bally J., Leventhal M., 1991, Nat 353, 234
Belloni T., Mendez M., King A., et al., 1997, ApJ 479, L145
Belloni T., Mendez M., King A., et al., 1997a, ApJ 488, L109
Boër M., Greiner, J., Motch, C., 1996, A&A 305, 835
Burgdorf M., Caux E., Clegg P., et al., 1997a, ESLAB preprint 97015, to be published in Advances in Space Research
Burgdorf M., Clegg P., Ewart D., et al., 1997b, in: Heras A., et al. (eds.), Proceedings 1^{st} ISO workshop on analytical spectroscopy, ESA SP-419, 51
Castro-Tirado A., 1996, in: Kouveliotou C., Briggs M., Fishman G. (eds.), Proceedings 3^{rd} GRB Symposium, AIP 384, 916
Castro-Tirado A., Brandt S., Lund N., 1992, IAU Circ. 5590
Castro-Tirado A., Geballe T., Lund N., 1996, ApJ 461, L99
Caux E., Gry C., 1997, in: Heras A., et al. (eds.), Proceedings 1^{st} ISO workshop on analytical spectroscopy, ESA SP-419, 253
Chaty, S., Mirabel I., Duc P., et al., 1996, A&A 310, 825
Chen W., Gehrels N., Leventhal M., 1994, ApJ 426, 586
Chen X., Swank J., Taam R., 1997, ApJ 477, L41
Clegg P., Ade P., Armand C., et al., 1996, A&A 315, L38
Durouchoux Ph., Corbel S., Wallyn P., et al., 1994, IAU Circ. 6000
Eikenberry, S., Fazio, G., 1995, IAU Circ. 6267
Eikenberry, S., Fazio, G., 1997, ApJ 475, L53
Eikenberry, S., Matthews K., Morgan E., et al., 1998, 191^{st} AAS Meeting, paper 100.08
Fender, R.P., Pooley G., Brocksopp C., et al., 1997, MNRAS 290, L65
Finoguenov A., Churazov E., Gilfanov M., et al., 1994, ApJ 424, 940
Genzel, R., Lutz D., Sturm E., et al., 1998, ApJ 498, 579
Ghigo, F., Waltman E., Foster R., 1995, IAU Circ. 6204
de Graauw T., Haser L., Beintema D., et al., 1996, A&A 315, L49
Greiner J., 1993, IAU Circ. 5786
Greiner J., Snowden S., Harmon B., et al., 1994, in: Fichtel C., Gehrels N., Norris J. (eds.), Proceedings 2^{nd} Compton Symposium AIP 304, 260
Greiner J., Morgan E., Remillard R., 1996, ApJ 473, L107
Grindlay J., 1994, ApJS 92, 465
Harmon B., Paciesas W., Fishman G., 1992, IAU Circ. 5619
Harmon B., Paciesas W., Fishman G., 1995, IAU Circ. 6204
Harmon B., Paciesas W., Zhang S., et al., 1995a, IAU Circ. 6266
Harmon B., Deal K., Paciesas W., Zhang S., et al., 1997, ApJ 477, L85
Hildebrand R., 1983, QJRAS 24, 267
v.d. Hucht K., Lutz D., Coté J., et al., 1994, ISO-SWS Observer's Manual, SRON/MPE Document ISO94-18, Issue 2.0, p. 21
Kessler M., Steinz J., Anderegg M., et al., 1996, A&A 315, L27
Kouveliotou C., Fishman G., Meegan C., et al., 1993, Nat 362, 728
Lutz, D., Feuchtgruber H., Genzel R., et al., 1996, A&A 315, L269
Malhotra S., Helou G., Stacey G., et al., 1997, ApJ 491, L27
Maloney P., Hollenbach D., Tielens A., 1996, ApJ 466, 561
Maloney P., Colgan S., Hollenbach D., 1997, ApJ 482, L41
Mirabel I., Rodriguez L., 1994, Nat 371, 46
Mirabel I., Rodriguez L., 1995, in: Böhringer H., Morfill, G., Trümper J. (eds.), Proceedings 17^{th} Texas Symposium, Annals of the New York Academy of Sciences 759, 21
Mirabel I., Rodriguez L., 1996, AP&SS 231, 54
Mirabel I., Rodriguez L., 1996a, in: Tsinganos K. (ed.), Solar and Astrophysical Magnetohydrodynamic Flows, Kluwer, p. 683
Mirabel I., Rodriguez L., Cordier L., et al., 1992, Nat 358, 215
Mirabel I., Duc P., Rodriguez L., et al., 1994, A&A 282, L17
Mirabel I., Rodriguez L., Chaty S., et al., 1996, ApJ 472, L111
Mirabel I., Bandyopadhyay R., Charles P., et al., 1997, ApJ 477, L45
Mirabel I., Dhawan V., Chaty S., et al., 1998, A&A 330, L9
Morgan E., Remillard R., Greiner J., 1996, IAU Circ. 6392
Morgan E., Remillard R., Greiner J., 1997, ApJ 482, 993
Nowak M., Wagoner R., Begelman M., et al., 1997, ApJ 477, L91
Paciesas W., Deal K., Harmon B., et al., 1996, A&AS 120, 205
Paul B., Agrawal P., Rao A., et al., 1997, A&A, 320, L37
Pooley G., 1996, IAU Circ. 6411
Pooley G., Fender, R., 1997, MNRAS 292, 925
Remillard R., Morgan E., Swank J., et al., 1997, IAU Circ. 6647
Robinson C., Zhang S., McCollough M., et al., 1997, IAU Circ. 6651
Rodriguez L., Mirabel I., 1997 ApJ 474, L123
Sams B., Eckart A., Sunyaev R., 1996, Nat 382, 47
Sams B., Sunyaev R., 1996a, IAU Circ. 6455
Sazonov S., Sunyaev R., 1995a, IAU Circ. 6196
Sazonov S., Sunyaev R., 1995b, IAU Circ. 6201
Sazonov S., Sunyaev R., 1995c, IAU Circ. 6209
Sazonov S., Sunyaev R., 1995d, IAU Circ. 6274
Scoville N., Kwan J., 1976, ApJ 206, 718
Stacey G., Viscuso P., Fuller C., et al., 1985, ApJ 289, 803
Sunyaev R., Churazov E., Gilfanov M., et al., 1991, ApJ 383, L49
Taam R., Chen X., Swank J., 1997, ApJ 485, L83
Waltman E., Foster R., Ghigo F., et al., 1995, IAU Circ. 6266
Zhang S., Harmon B., Paciesas W., et al., 1995, IAU Circ. 6209
Zhang N., Robinson C., Harmon B., et al., 1996, IAU Circ. 6411